Dense volumetric velocity field reconstruction with time-segment assimilation

Gabriel González[1]*, Andrea Sciacchitano[1], Fulvio Scarano[1]

[1] Delft University of Technology, Department of Aerospace Engineering, Delft, The Netherlands

* G.GonzalezSaiz@tudelft.nl

Abstract

The time-segment assimilation (TSA) method levers upon the spatio-temporal information from a finite number of successive time samples of particle velocity, coming from PTV and STB, into a refined spatial reconstruction of the velocity field of the flow. The method recently introduced by Schneiders and Scarano (2018) is elaborated here further in its working principle and hypotheses. Three regimes of operation are identified, with respect to the normalized length of the time segment, of which, the adjacent tracks regime is found to be the most promising in terms of spatial resolution and computational viability. The ability of TSA in delivering high-resolution velocity reconstructions is inquired by a numerical and experimental assessment. The numerical study is based upon a synthetic field of a 3D sine-wave lattice, popular among previous works. The amplitude modulation of sinusoids appears to be increased when moving from the assimilation of a short time sequence, towards a longer time segment. Furthermore, it is observed that the result of the numerical process is independent of the time interval chosen for time-marching, provided that the CFL condition is respected. The experimental analysis regards experimental data from a multichannel swirling jet. The initial results demonstrate that a richer vorticity field can be retrieved when the assimilation is conducted with time segments that approach the stringy regime.

1   Introduction

Tomographic particle image velocimetry (TOMO-PIV, Elsinga *et al.*, 2006) has been widely adopted for volumetric velocity flow measurements after its introduction. The method relies upon voxels discretization and 3D spatial cross-correlation analysis, whereby interrogation volumes must include approximately 5-20 particles. The dense velocity field is obtained on a Cartesian grid defined by the interrogation boxes and the overlap factor. In the Lagrangian particle tracking approaches (LPT, Malik *et al.*, 1993), scattered velocity measurements are obtained at instantaneous particle locations, avoiding the spatial filtering effect of the cross-correlation technique. For the time-resolved tomographic PTV (Novara and Scarano, 2013), more accurate velocities are obtained with the information of the particle trajectories.

However, for an accurate reconstruction of the particles by these image-based techniques, there is a limitation on the maximum density of particles imaged on the sensors, quantified in particles per pixel (ppp). This limit was 0.025 ppp for a three standard camera system in tomographic PIV (Elsinga *et al.*, 2006) and 0.005 ppp for volumetric PTV (Maas *et al.*, 1993). Recent advancements, such as the iterative particle reconstruction (IPR, Wieneke 2012) triangulation method and the Shake-the-Box technique (Schanz *et al.*, 2016) have significantly advanced the limit on image density for an accurate tracking of particles to that of tomographic PIV to the range 0.05 – 0.1 ppp. Overall, the restriction on

the seeding concentration of the tracer particles draws a limit on the achievable spatial resolution from PIV and PTV volumetric measurements, that becomes more evident when measuring small scales in large-scale measurements with HFSB (Bosbach *et al.*, 2009; Scarano *et al.*, 2015).

Data assimilation techniques are increasingly used to enhance the temporal and spatial resolution in flow measurements by 2D or 3D PIV. By enforcing the compliance of the measured instantaneous flow information (velocity and its material derivative) with the governing equations of fluid motion (conservation of mass and momentum), such techniques enable resolving flow scales smaller than the average inter-particle distance (Schneiders and Scarano, 2016; Gesemann *et al.*, 2016) and have shown ability to capture processes, such as vorticity fluctuations dynamics and turbulent kinetic energy dissipation, taking place at the right side of the scales spectrum (Schneiders *et al.*, 2017). Most of the proposed approaches perform the assimilation on the basis of an instantaneous flow measurement (e.g. velocity, vorticity, acceleration).

However, a great potential resides in the information of the complete tracks followed by the particles, and could further increase the spatial resolution of the measurements with respect to previous techniques. This concept of assimilating measurements comprising a finite time interval, as obtained from time-resolved experiments, has been introduced recently by Schneiders and Scarano (2016, 2018) as time-segment assimilation (TSA). The latter is particularly meant for applications to time-resolved data of sparse tracers distributions obtained from volumetric particle tracking techniques such as tomographic PTV (Novara and Scarano, 2013) and Shake-the-Box (Schanz *et al.*, 2016). Some discussion of the features and performances TSA technique has been given, based on a simplified synthetic PTV experiment using a steady 3D lattice of sinusoids (Schneiders and Scarano, 2018). An interesting trend showed the potential increase of the spatial resolution with the length of the assimilated time segment. It was not clear, however, to what extent, elongation of the time segment length would give benefits in terms of spatial resolution, neither the working regimes of TSA have been elucidated.

To advance the understanding of TSA, we perform a detailed analysis of the TSA spatial response, in comparison with other reported techniques (interpolators and spatial filters). Furthermore, to understand the potential for application to experimental data with the associated measurement uncertainties, the TSA technique is applied for the analysis of turbulent shear flows. In particular, the data from a multichannel swirling jet experiment from Ianiro *et al.* (2018) is used.

2   Working principle of TSA and underlying hypotheses

Particle tracers immersed in the fluid flow are assumed to be homogeneously distributed in space. Their concentration C is defined as the number of particles present in a unit volume. The concentration of particle tracers directly determines the length-scales of the flow that can be instantaneously resolved as discussed in previous literature (VIC+, Schneiders and Scarano, 2016; FlowFit, Gesemann *et al.*, 2016).

Consider a three dimensional flow schematically depicted in Fig. 1. Three tracer particles $[p_1, p_2, p_3]$ are captured at a given time t_0 (red solid outline circles). Such particles follow the trajectories $[\Gamma_1, \Gamma_2, \Gamma_3]$, (solid blue lines). Provided that the measurement of the particles position is obtained in time-resolved mode (e.g. by means of high-repetition rate PIV equipment), the sampled positions at consecutive times $[t_0, t_1, t_2, \dots t_{Nt}]$ separated by the sampling time interval Δt_s are shown by dashed outline red circles. We denote the overall time segment encompassed by the N samples as $\mathcal{T} = $

$[0, \Delta t_s Nt]$. The finite-length curve determined by the N positions is denoted as a track (represented by solid black lines in *Figure 1-right*).
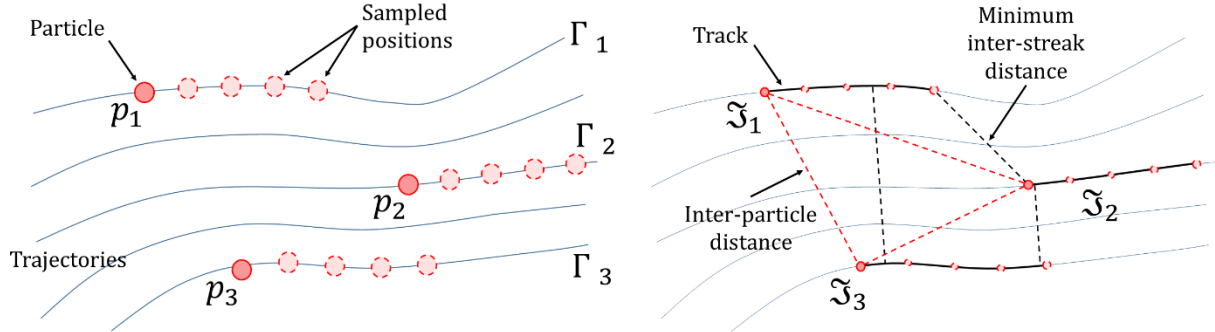

Figure 1 - Left: schematic of tracer particles (*red*) sampled in their motion along trajectories (*solid blue*). Samples at time t_0 are represented by red circles with solid outline. Subsequent particle samples are marked by dashed outline. *Right*: distance between neighbouring particles at time instance t_1 (*dashed red*) and minimum distance between tracks (*dashed black*). Tracks are represented as solid black lines.

When the flow velocity is inferred from the analysis of the motion of individual tracers (e.g. PTV, Malik *et al.*, 1993), the velocity field measurement must be obtained by means of spatial interpolation. The spatial resolution depends upon the instantaneous concentration of tracer particles as well as the scheme used to interpolate between the scattered data points. Let us denote the average distance between neighbouring particles at time t_0, by $\bar{r}_0$.

For a homogeneous concentration, the average inter-particle distance evaluated on a large ensemble of particles is independent of time and of the length of the time segment $\mathcal{T}$.

Recent data assimilation methods (*VIC+,* Schneiders and Scarano, 2016; *Flowfit,* Gesemann *et al.*, 2016), make use of the instantaneous velocity and acceleration for the assimilation of the instantaneous volumetric velocity field, to retrieve smaller flow scales than the inter-particle distance. In the above methods, however, the instantaneous concentration and the related inter-particle distance determine the maximum spatial resolution that can be achieved.

Let us consider now the tracks $[\mathfrak{I}_1, \mathfrak{I}_2, \ldots \mathfrak{I}_M]$ followed by the particles $[p_1, p_2, \ldots p_M]$ for the time segment $\mathcal{T}$. We can focus our attention to the distance between tracks instead. The inter-track distance $\tilde{r}$, shown with dashed black lines in Fig. 1-*right* depends not only upon the inter-particle distance, but also on the path traveled during $\mathcal{T}$. In particular, the condition $\tilde{r} < \bar{r}_0$ holds true at all times and everywhere in the observed flow domain.

The inter-streak distance has the following property with time: if the length of the time segment $\mathcal{L}_{track}$ is much shorter than the inter-particle distance then $\tilde{r} \sim \bar{r}_0$; if, instead $\mathcal{L}_{track}$ is significantly longer than the inter-particle distance then $\tilde{r} << \bar{r}_0$. The latter concept is illustrated in Fig. 2.

Following the above reasoning, the working hypothesis of the time-segment assimilation (TSA) shifts the dependency of spatial resolution from the inter-particle distance to the inter-track distance. As a consequence, the length of the time segment assimilated $\mathcal{T}_s$ is the parameter determining such shift. Three different regimes can be foreseen and are depicted in Fig. 2. The TSA technique is based on time-resolved recordings of the particle positions along their trajectories[1].

---

[1] In a time-resolved measurement of particles motion, the displacement occurring between subsequent recordings is small enough that the linearized trajectory of the tracer is a good approximation of the exact trajectory.

$$\begin{cases} \bar{r} \gg \mathcal{L}_{track} : streaked\ particles\ regime \\ \bar{r} \cong \mathcal{L}_{track} : adjacent\ tracks\ regime \\ \bar{r} \ll \mathcal{L}_{track} : stringy\ tracks\ regime \end{cases} \qquad (1)$$
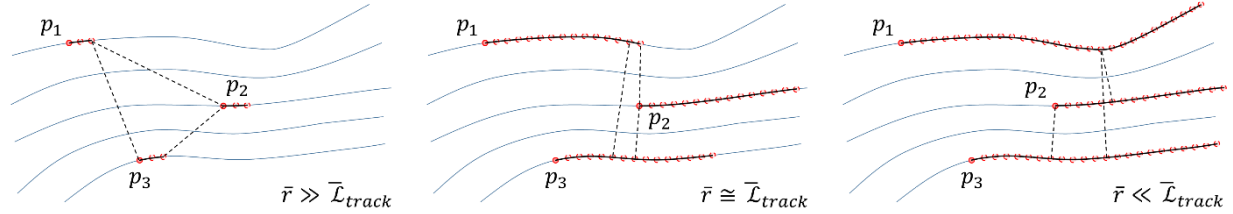

Figure 2 - Inter-streak distance (*dashed black*) between tracks (*bold black*) for the streaked-particles regime (*left*), adjacent-tracks regime (*middle*) and the stringy-tracks regime (*right*).

With a short time segment (for instance given by only three time samples, in Fig. 2-*left*) the average inter-track distance differs very little from the inter-particle distance and the spatial resolution is expected to be similar to that of methods based on the instantaneous flow properties. On the other side of the spectrum, for extremely long tracks (stringy tracks regime, Fig. 2-*right*), the distance between neighbouring tracks has reached its minimum and the spatial resolution is expected to be more similar to that obtained at higher tracers concentration. An intermediate regime is identified as a potential optimum considering the computational efficiency of the calculations, where the track length is sufficient to approach the above minimum. This regime is denoted as adjacent tracks regime. The following sections aim to prove the stated rationale: the accuracy of the flow reconstruction with TSA depends upon the inter-track distance, and hence the regimes defined above. The temporal separation between the samples used for the assimilated time segment, is initially considered small enough for the reconstruction not to show dependence on it. This condition reads as:

$$\tau = \frac{U\ T_s}{\bar{r}} \sim 1 \qquad (2)$$

where U is a reference velocity of the flow, T_s is the length of the time segment, and $\bar{r}$ is the average inter-particle distance.

3   Methodology

The aim of the TSA technique is to calculate the vorticity field that fits best the flow at a given instant and its past and future times, i.e. the time-segment. The current implementation was already presented by Schneiders and Scarano (2018). The entire procedure is sketched by Fig. 3 and will be referred by the description developed in the following section.

The input of the current technique are time-resolved tracked data from tomographic PTV (Novara and Scarano, 2013) or Shake-the-Box algorithm (Schanz *et al.*, 2016), that is a set of spatially scattered velocity measurements at regularly spaced time intervals. The sampling frequency of the experimental data is usually assumed high enough to resolve temporally the relevant flow scales of the problem.
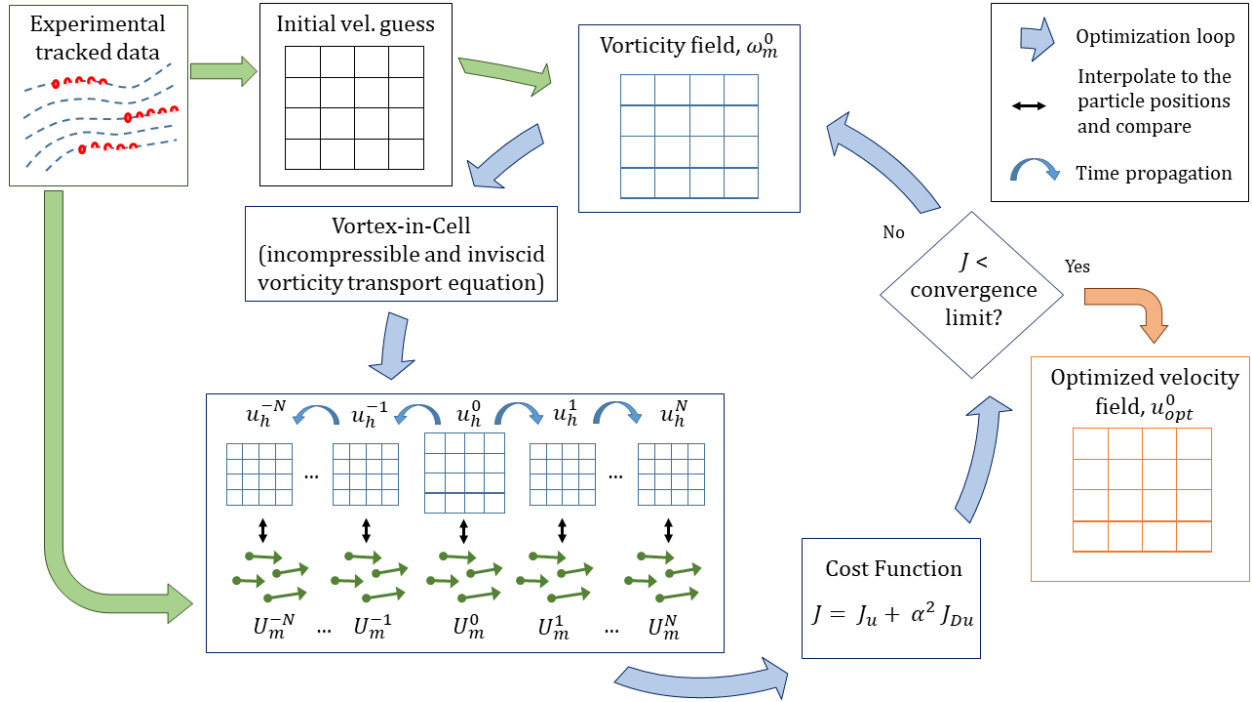
Figure 3 - Schematic of Time-Segment Assimilation (TSA) reconstruction framework. An optimization loop (*blue*) is started with a rough estimate of the vorticity field at the centre of the time segment, interpolated from the measurements (*green*). The vorticity is marched in time with the VIC methodology and a cost function is calculated from the differences between the marched velocities and the measurements. The process is iterated until the cost function is small enough and the optimized velocity field (*orange*) at t_0 is obtained.

The optimization process is based on the Vortex-in-Cell framework (Christiansen, 1973), similarly to the VIC+ methodology (Schneiders and Scarano, 2016). Therefore, a vortex-particle discretization is used for the numerical integration of the vorticity field, from which the velocity field at every instant of the assimilated time-segment is calculated by solving the Poisson equation. The governing equation of the flow was taken to be the incompressible and inviscid vorticity transport equation,

$$\frac{\partial \boldsymbol{\omega}}{\partial t} = (\boldsymbol{\omega} \cdot \nabla) \boldsymbol{u} + (\boldsymbol{u} \cdot \nabla) \boldsymbol{\omega} \tag{3}$$

Then, the velocity from the dense grid is interpolated back to the particle positions to calculate the differences between the measurement tracked data and the numerical velocity at every sampled instant of the track. The differences on velocity, $\boldsymbol{u}$ and material derivative of velocity, $D\boldsymbol{u}/Dt$ comprise the cost function.

An iterative problem is built upon these steps to minimize the cost function, sketched with blue arrows in Fig. 3, by tuning the optimization variable, the gridded vorticity, in every iteration. It is solved using the limited-memory Broyden-Fletcher-Goldfarb-Shanno method (L-BFGS, Liu and Nocedal 1989), an approximation of the BFGS, a quasi-Newton method approach, with a limited amount of memory.

4   Numerical assessment

A synthetic flow field is generated for the numerical assessment of the TSA technique. The field is described by the unsteady 3D sine wave lattice shown below,

$$\begin{cases} u = A \, sin\left(\frac{2\pi x}{\lambda}\right) sin\left(\frac{2\pi y}{\lambda}\right) \\ v = A \, cos\left(\frac{2\pi x}{\lambda}\right) cos\left(\frac{2\pi y}{\lambda}\right) \\ w = A \end{cases} \tag{4}$$

where A is the amplitude of the waves, λ is the wavelength and x, y and z are the Cartesian coordinates. This reference function was already used in previous works for steady numerical assessments (Willert and Gharib, 1991; Scarano and Riethmuller, 2000; Schrijer and Scarano, 2008; Scarano, 2003; Schneiders and Scarano, 2016). A simulated volume is considered with a length of 2λ in every direction, 0.4x0.4x0.8 m³, where a uniform concentration of particles is generated in a pseudo-random process and propagated according to the underlying synthetic velocity field. No particle reconstruction errors are simulated. For the calculation of the particle motion, a fourth-order Runge-Kutta method was chosen. In order to keep a constant and quasi-homogeneous concentration within the volume and time period of simulation, the amount of particles that exit the flow through the outlet boundaries at a given time instant are generated with the same velocity distribution close to the opposite inlet boundary of the domain at the next time step, resembling periodic boundary conditions.

A spatial response analysis is carried out for the mentioned velocity field varying the concentration of particles generated, C, and the number of samples composing the assimilated time segment, Nt. The TSA method is applied with the shortest duration of observation (3 snapshots to have a central temporal scheme), a long segment, Nt =11, and a significantly long segment, Nt = 31. The non-dimensional time lengths of these segments are representative of the three regimes explained section 2. For a time separation between samples $\Delta t_{sampling} = 0.01$ s, a convection velocity of the particles $A = 2$ m/s and an average inter-particle distance $\bar{r} = \sqrt[3]{(3/4\pi \; 1/C)} \in (0.03, 0.08)$ m, the non-dimensional time τ is $\tau \in (0.1, 0.4), (0.55,1.5), (1.55, 4.1)$ for Nt=3, 11, 15 respectively. For the current analysis, the grid spacing used for the TSA reconstruction is kept constant for the different cases, $h = 0.01 \; m$.

For a first qualitative analysis of the TSA spatial response, Fig. 4 shows the averaged reconstructed vertical velocity component for the normalized average inter-particle distances $\bar{r} = 0.08, 0.05, 0.03$. A vertical projection of the particles considered in the simulated three-dimensional domain is given in the first row. The reference field at the right presents the sine waves pattern from Eq. (4). The results clearly show the general trend of retrieving more peaks and with higher values as the assimilation considers a longer time. In addition, it must be pointed out that the TSA approach is capable to reconstruct extremely sparsely seeded flows by using long assimilation times for the reconstruction, as it is the case of $\bar{r} = 0.08$ for 31 samples, where the sign of the lobes is already found with a few particles in the domain. On the other hand, when the tracked data is sufficiently dense, the technique does not show considerable improvements between different lengths of the assimilated time-segments, reaching even the point of overestimating the peak velocity values.
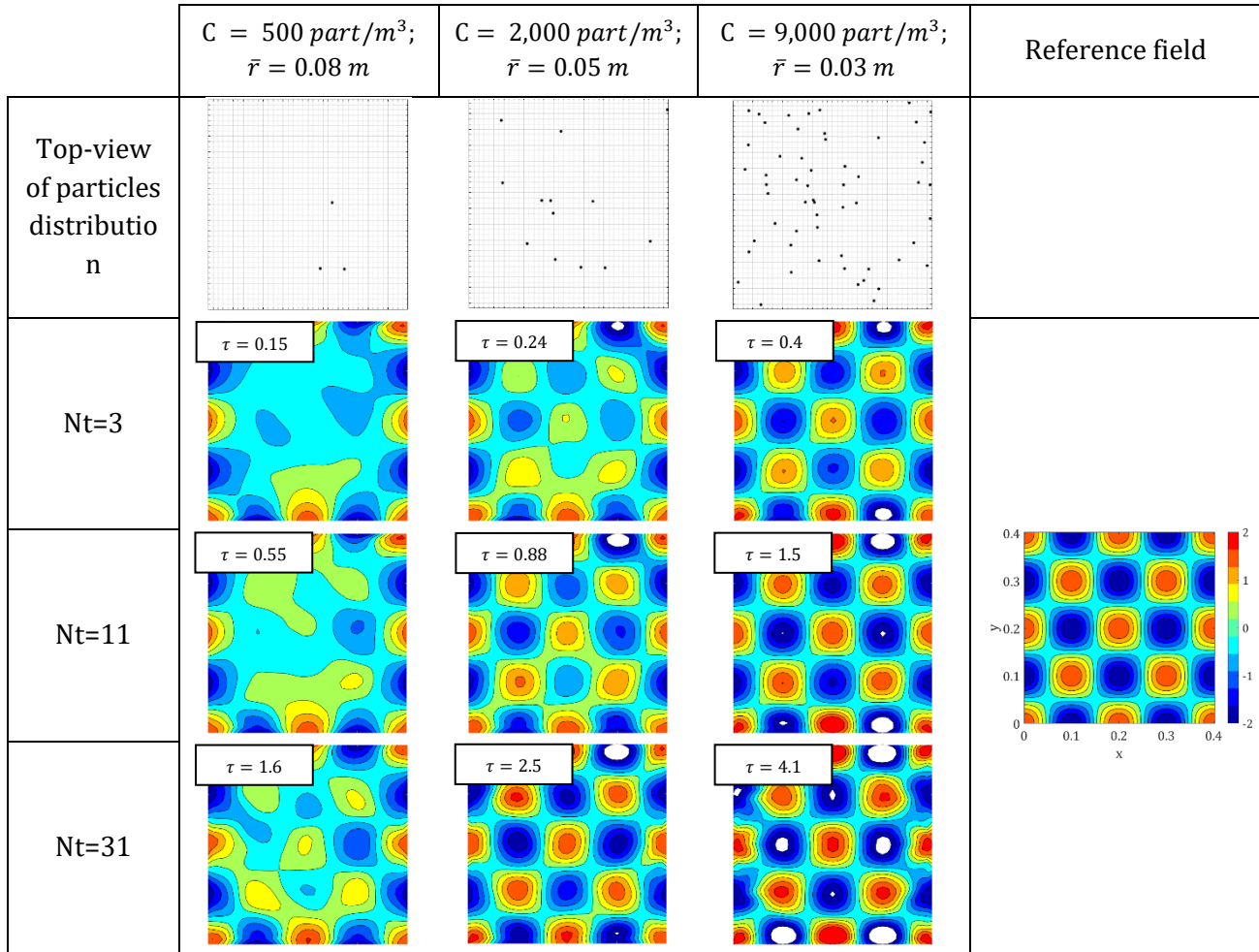
$C = 500 \, part/m^3$; $\bar{r} = 0.08 \, m$	$C = 2,000 \, part/m^3$; $\bar{r} = 0.05 \, m$	$C = 9,000 \, part/m^3$; $\bar{r} = 0.03 \, m$	Reference field
Top-view of particles distribution			
Nt=3			
Nt=11			
Nt=31			

Figure 4 - Starting from the top, top-view of particles distribution in the simulation domain, reconstructed u-component of the velocity field for 3 time samples, 11 time samples and 31 time samples. From left to right, concentrations of 500 particles/m³, 2000 particles/m³ and 9000 particles/m³. Reference *u* velocity field shown on the right.

Figure 5-*left* shows the amplitude modulation evaluated with three time-segments. The spatial response of a top-hat sliding average (denoted as linear filter) over a cubic element containing 10 tracer particles is also shown for reference. The horizontal axis represents the normalized wavenumber *r**, computed as the ratio between the average inter-particle distance and the flow wavelength $r^* = \bar{r}/\lambda$ (lower axis), or between the linear size of the cubic element used as linear filter and the flow wavelength (*l** on the upper axis). The amplitude modulation *u** is defined as the ratio between the reconstructed velocity and the exact value at the peak locations of the analytical field. The coloured regions around the main curves indicate the standard deviation when averaging the field peaks differences for different vertical planes of the volume; for the current analysis, a number of planes $Nplanes = 50$ with 9 peaks each were considered.

The results show a similar behaviour as that observed in Schneiders and Scarano (2018); increasing the time segment yields some systematic shift of the roll-off point (*u** = 0.5) towards higher values of *r** (viz. smaller length scales). Moreover, the TSA technique shows generally a flat response that decreases to the cut-off wavelength of $r^* = 0.2, 0.27$ for 3 and 11 snapshots assimilation. The longest

segment presents a flatter region with a cut-off at $r^* = 0.35$ with the drawback of overshooting by 6.5% the reference value.
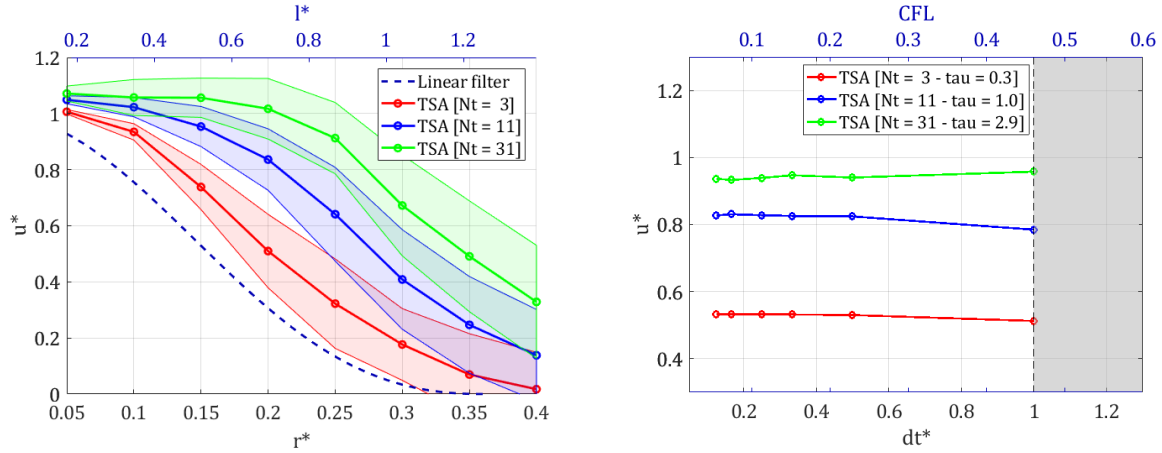

Figure 5 - Amplitude modulation for the TSA technique (time segments with 3, 11 and 31 samples) varying the seeding concentration (*left*) and the internal time separation of the VIC methodology (*right*).

An additional analysis on the effect of the internal time integration is carried out for the same three time segments at a seeding concentration of $C \cong 300$ particles/m³, and normalized inter-particle distance $r^* = 0.21$. Fig. 5-*right* shows the amplitude modulation of the reconstructions for the normalized time-marching frequency, $dt^* = \Delta t_{marching}/\Delta t_{sampling}$. The CFL computed from the reference velocity $A = 2$ m/s and grid spacing $h = 0.01$ m is given as top x-axis. The operation of the technique appears to be independent of the choice on the internal time separation for the given conditions, i.e. CFL lower than unity.

5   Experimental assessment

The experimental case considered for TSA analysis regards a multichannel swirling jet flow documented by Ianiro *et al.* (2018). The experiment considers a water multichannel swirling jet with an average exit velocity of 0.05 m/s and a Reynolds number Re=1000. The jet, exiting from a 19.7 millimetre nozzle at the bottom wall of a transparent octagonal water tank with full optical access from the walls, was recorded with three LaVision Imager Pro HS CMOS cameras. The flow was seeded with a constant concentration of micrometric polyamide particles and was illuminated by a solid-state diode-pumped Quantronix Darwin-Duo Nd-YLF laser and recorded at a rate of 100 Hz.

Table 1. Tomographic PIV setup.

Seeding	Polyamide, 56 µm diameter
Recording devices	LaVision Imager Pro HS CMOS ($2016 \times 2016\ px^2$, $11\ \mu m$ pixel size)
Illumination	Quantronix Darwin-Duo Nd-YLF laser (2x25 mJ at 1 kHz)
Imaging	M=0.205;
Measurement domain	$86 \times 43 \times 43\ mm^3$ in $160 \times 80 \times 80$ voxels
Number of samples	200

The original tomographic PIV measurements by Ianiro *et al.* (2018) were processed with one of the latest correlation PIV techniques, the sequential motion-tracking-enhanced MART (SMTE, Lynch and Scarano 2015) for the volumetric reconstruction. The three-dimensional motion of the particles was performed with the fluid trajectory correlation (FTC, Lynch and Scarano 2013) using interrogation windows of $40 \times 40 \times 40$ voxels ($2.1 \times 2.1 \times 2.1$ mm³) with 75% overlap. The vector pitch was approximately 0.5 mm.

For the current analysis, raw images were reprocessed using the PTV technique. The volumetric self-calibration was recalculated from pre-processed run, resulting in an average disparity of 0.03 pixels, very similar to the former disparity. The triangulation of the particles positions in time and their velocities were calculated by means of the iterative particle reconstruction (IPR, Wieneke 2013) technique and the tracking algorithm Shake-the-Box (STB, Schanz *et al.*, 2016) was applied. For the particle tracking itself, a nine-snapshot track length and a third order polynomial for the track fitting were selected.
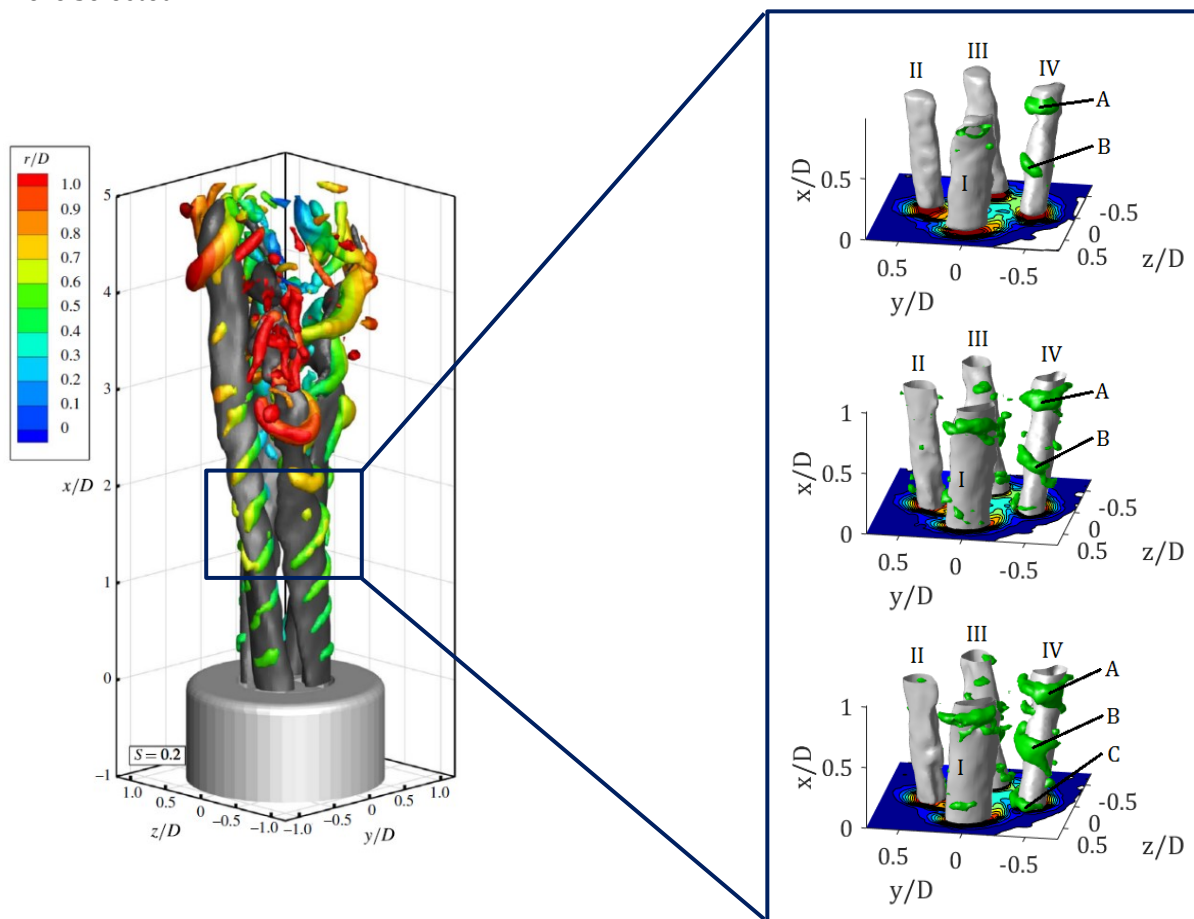

Figure 6 - (*Right*) Iso-surfaces of instantaneous velocity magnitude (*grey*, $U / U_e = 0.8$) and Q-criterion (*green*, $Q \cdot D^2 / U_e^2 = 7$) for a three-dimensional linear interpolation (*top*), TSA reconstruction with three time samples (*middle*), and TSA reconstruction with 13 time samples (*bottom*). (Left) Instantaneous flow field at $S = 0.2$ from Ianiro *et al.* (2018).

Regarding the TSA post-processing, a part of the overall measured volume was extracted for the analysis, resulting in a computational domain of $0.03 \times 0.04 \times 0.03$ m³. The computational grid coincides with the vector pitch of the PIV processing for a meaningful comparison. The maximum velocity of the particles in the reduced volume was found to be $U_e = 0.06$ m/s, so the internal time separation for the algorithm was chosen as $\Delta t_{marching} = 0.05$ s to comply with the CFL condition. The

time separation between samples was kept as the inverse of the sampling frequency of the measurement itself, $\Delta t_{sampling} = 0.01$ s. A three-dimensional qualitative comparison of the instantaneous flow organization between the different techniques is given in Fig. 6. Iso-surfaces of velocity (in grey) and Q-criterion (in green) are shown for two TSA cases, time-segment lengths of 3 and 11 time samples, and a linear interpolation in space of the particles onto the Cartesian grid used for the TSA technique.

The multichannel swirling jet was produced by means of four vanes at the exit of the nozzle imparting the swirl to the flow, resulting on four high velocity columns, named in Fig. 6 as I, II, III and IV. The vorticity is arranged in shape of helices that surround the outer part of each of the jet sections (Ianiro *et al.*, 2018).

Drawing the attention to the velocity column IV, it is noticeable that the time segment length of the assimilation adds to the reconstruction of the spatial velocity and vorticity distributions. In the case of the linear interpolation, the structures A and B are only partially captured. When applying the TSA technique with a 3-samples segment (Fig. 6 *mid-right*), a richer vorticity field is retrieved. Structures A and B seem to embrace the velocity column and secondary structures can be visualized. As hypothesised in section 2, the adjacent tracks regime yields the richest recovery of coherent structures with respect to the rest of the configurations analysed. In this particular case, with an assimilation of 13 time samples (Fig. 6 *bot-right*), the structures A and B are more well defined and an additional structure C appears upstream.

6 Conclusions

Time-segment assimilation is a recent data assimilation technique that considers the length of a finite time-segment to reconstruct the optimal vorticity and velocity fields described by such segment. Both numerical and experimental analyses were carried out in order to understand further the advantages and limitations of this methodology.

From the numerical tests with synthetic data, it is clear that the time-segment assimilation technique enables resolving flow scales two to three times smaller than standard correlation analysis. The longer times considered for assimilation improve the spatial resolution of the reconstruction with the TSA technique. Thus, the technique shows great potential especially for scarcely seeded flow measurements, such as those carried out by large-scale PIV with Helium-filled soap bubbles as flow tracers. Furthermore, the performance of the internal time marching of the technique is independent of the CFL condition if the CFL number is lower than unity. At high seeding concentrations, the TSA technique returns an overshoot of the actual velocity amplitude, which increases with the length of the assimilated time segment and is yet to be explained.

An experimental analysis is performed on jet experimental data where two assimilations with different time-segment lengths were compared to a trilinear interpolation of the sparse data. Results strengthen the conclusions from the numerical study; the longer the temporal streak considered in the reconstruction, the richer the field of coherent structures that is obtained.

Acknowledgements

References

Bosbach J, Kühn M, Wagner C (2009). Large scale particle image velocimetry with helium filled soap bubbles. *Experiments in fluids. 46(3):539-47.*

Christiansen IP (1973). Numerical simulation of hydrodynamics by the method of point vortices. *Journal of Computational Physics. 13(3):363-79.*

Elsinga GE, Scarano F, Wieneke B, van Oudheusden BW (2006). Tomographic particle image velocimetry. *Experiments in fluids. 41(6):933-47.*

Ianiro A, Lynch KP, Violato D, Cardone G, Scarano F (2018). Three-dimensional organization and dynamics of vortices in multichannel swirling jets*. Journal of Fluid Mechanics. 843:180-210*.

Gesemann S, Huhn F, Schanz D, Schröder A (2016). From noisy particle tracks to velocity, acceleration and pressure fields using B-splines and penalties. *18th Int. Symp. Appl. Laser Imaging Tech. Fluid. Mech., Lisbon, Portugal*

Lynch KP, Scarano F (2015). An efficient and accurate approach to MTE-MART for time-resolved tomographic PIV. *Experiments in Fluids. 56(3):66.*

Lynch K, Scarano F (2013). A high-order time-accurate interrogation method for time-resolved PIV. *Measurement Science and Technology. 24(3):035305.*

Liu DC, Nocedal J (1989). On the limited memory BFGS method for large scale optimization. *Mathematical programming. 45(1-3):503-28.*

Maas HG, Gruen A, Papantoniou D (1993). Particle tracking velocimetry in three-dimensional flows. *Experiments in fluids. 15(2):133-46*.

Malik NA, Dracos T, Papantoniou DA (1993). Particle tracking velocimetry in three-dimensional flows. *Experiments in Fluids. 15(4-5):279-94*.

Novara M, Scarano F (2013). A particle-tracking approach for accurate material derivative measurements with tomographic PIV. *Experiments in fluids. 54(8):1584.*

Scarano F, Riethmuller ML (2000). Advances in iterative multigrid PIV image processing. *Experiments in Fluids. 29(1):S051-60.*

Scarano F (2003). Theory of non-isotropic spatial resolution in PIV. *Experiments in Fluids. 35(3):268-77.*

Scarano F, Ghaemi S, Caridi GC, Bosbach J, Dierksheide U, Sciacchitano A (2015). On the use of helium-filled soap bubbles for large-scale tomographic PIV in wind tunnel experiments. *Experiments in Fluids. 56(2):42.*

Schanz D, Gesemann S, Schröder A (2016). Shake-The-Box: Lagrangian particle tracking at high particle image densities. *Experiments in fluids. 57(5):70.*

Schrijer FF, Scarano F (2008). Effect of predictor–corrector filtering on the stability and spatial resolution of iterative PIV interrogation. *Experiments in fluids. 45(5):927-41.*

Schneiders, Scarano (2016) Dense velocity reconstruction from tomographic PTV with material derivatives. *Experiments in Fluids. 57:139.*

Schneiders, Scarano, Elsinga (2017). Resolving vorticity and dissipation in a turbulent boundary layer by tomographic PTV and VIC+. *Experiments in Fluids. 58:27.*

Schneiders JF, Scarano F (2018). On the use of full particle trajectories and vorticity transport for dense velocity field reconstruction*. 19th Int. Symp. Appl. Laser Imaging Tech. Fluid. Mech., Lisbon, Portugal*

Wieneke B (2012). Iterative reconstruction of volumetric particle distribution. *Measurement Science and Technology. 24(2):024008.*

Willert CE, Gharib M (1991). Digital particle image velocimetry. *Experiments in fluids. 10(4):181-93.*